IOSR Journal of Dental and Medical Sciences (IOSR-JDMS)
e-ISSN: 2279-0853, p-ISSN: 2279-0861.Volume 25, Issue 10 Ser. 5 (October. 2026), PP 37-44
www.iosrjournals.org

Role of Multi-Slice Computed Tomography in the Evaluation of Paranasal Sinus Diseases: A Hospital-Based Descriptive Cross-Sectional Study

Hawa Begum[1]*, Biplob Mondal[2], Rafeza Khanom[3], Mithun Bahadur[4], Sabbir Hossen[5]

[1] *Associate Professor, Department of Radiology and Imaging, Sher-e-Bangla Medical College & Hospital (SBMCH), Barishal, Bangladesh.*
[2] *Radiologist, Department of Radiology and Imaging, Sher-e-Bangla Medical College & Hospital (SBMCH), Barishal, Bangladesh.*
[3] *Radiologist, Department of Radiology and Imaging, Shaheed Suhrawardy Medical College & Hospital (ShSMCH), Dhaka, Bangladesh.*
[4] *Emergency Medical Officer (EMO), Upazila Health Complex (UHC) Tazumuddin, Bhola, Bangladesh.*
[5] *Medical Officer, Institute of Nuclear Medicine and Allied Sciences (INMAS), Barishal, Bangladesh.*
**** Corresponding Author:** Dr. Hawa Begum, Associate Professor, Department of Radiology and Imaging, Sher-e-Bangla Medical College & Hospital (SBMCH), Barishal-8200, Bangladesh.*

ABSTRACT
***Background:** Paranasal sinus pathologies are major indications for cross-sectional imaging referral. Multi-Slice Computed Tomography (MSCT) provides multiplanar visualization of mucosal disease, drainage pathways, and osseous landmarks. This study aimed to characterize sinonasal pathologies, determine anatomical variations, and evaluate mucosal opacification using Lund-Mackay CT staging in southern coastal Bangladesh.*
***Methods:** This hospital-based, descriptive cross-sectional study evaluated N = 126 consecutive symptomatic patients undergoing high-resolution helical MSCT at Sher-e-Bangla Medical College Hospital, Barishal (January–December 2025). Chronic rhinosinusitis (CRS) cases (n = 96) were staged via Lund-Mackay scores categorized into study-specific opacification tiers (mild: 1–6, moderate: 7–12, severe: 13–24). Data were analyzed using SPSS Version 28.0.*
***Results:** Mean age was 34.6 ± 12.4 years with male predominance (57.9%, n = 73). Nasal obstruction (77.8%, n = 98) and facial headache/pain (66.7%, n = 84) were the leading symptoms. Prevalent variations included deviated nasal septum (62.7%, n = 79), Agger nasi cells (41.3%, n = 52), concha bullosa (34.1%, n = 43), Haller cells (14.3%, n = 18), and Onodi cells (8.7%, n = 11). Maxillary (80.2%, n = 101) and anterior ethmoid (61.9%, n = 78) sinuses were predominantly affected. Mucosal thickening occurred in 82.5% (n = 104) and ostiomeatal occlusion in 56.3% (n = 71). Mean Lund-Mackay score was 10.8 ± 4.2.*
***Conclusion:** MSCT provides detailed anatomical mapping of mucosal disease and critical structural variants, establishing an essential pre-operative roadmap that assists in mitigating surgical complications during Functional Endoscopic Sinus Surgery.*
***Keywords:** Multi-Slice Computed Tomography; Paranasal Sinuses; Chronic Rhinosinusitis; Anatomical Variations; Ostiomeatal Complex; Functional Endoscopic Sinus Surgery; Lund-Mackay Staging*

I. INTRODUCTION

Paranasal sinus diseases, predominantly chronic rhinosinusitis (CRS) and sinonasal polyposis, represent a widespread healthcare burden affecting approximately 10% to 15% of the adult population worldwide [1, 2]. Clinical manifestations, including persistent nasal congestion, facial pain, mucopurulent rhinorrhea, and olfactory reduction, lead to substantial functional impairment, sleep disruption, and decreased occupational productivity [3, 4]. Pathophysiologically, sustained sinonasal inflammation stems from impaired mucociliary transport, osteomeatal unit occlusion, and localized ventilation deficits within the paranasal cavities [5].

Diagnostic assessment historically relied on conventional plain skull radiography, including Waters' and Caldwell projections. However, planar radiography exhibits pronounced diagnostic limitations, primarily attributable to the structural overlap of complex facial bones, inadequate soft-tissue differentiation, and poor sensitivity for early mucosal disease [6]. Planar radiographs fail to visualize the delicate architectural subunits of the ostiomeatal complex (OMC), anterior ethmoid cells, and sphenoethmoidal recesses, frequently yielding false-negative findings that misguide surgical decision-making [7].

Multi-Slice Computed Tomography (MSCT) has superseded planar imaging as the imaging reference standard for sinonasal disease, providing isotropic sub-millimeter multiplanar reformations in axial, coronal, and

sagittal planes [8]. High-resolution coronal reformations directly mirror the endonasal optical perspective of the operating otolaryngologist, enabling precise delineation of drainage pathways and bone-mucosa interfaces [9]. Pre-operative MSCT mapping is mandatory before Functional Endoscopic Sinus Surgery (FESS) to recognize hazardous anatomical variants—such as Onodi cells, Haller cells, prominent Agger nasi cells, and deep olfactory fossae (Keros classification)—that heighten the risk of orbital entry, skull base injury, cerebrospinal fluid leaks, and severe vascular trauma [10, 11]. Standardized Lund-Mackay CT staging further quantifies mucosal disease severity to guide clinical interventions [12].

In southern coastal Bangladesh, tertiary medical centers encounter a substantial burden of chronic sinonasal presentations within an agrarian demographic [3, 13]. Despite high clinical referral rates at Sher-e-Bangla Medical College Hospital in Barishal, systematic documentation integrating MSCT disease patterns with surgical danger landmarks remains limited for this population. Detailed multiplanar imaging characterization is vital to provide local otolaryngologists with reliable anatomical guidance and baseline epidemiological metrics. This study was undertaken to characterize the radiological spectrum of paranasal sinus pathologies, determine the prevalence of predisposing anatomical variations, and evaluate inflammatory extent via standardized Lund-Mackay CT staging in this regional tertiary referral cohort.

II. METHODS

This hospital-based, descriptive cross-sectional study was conducted at the Department of Radiology & Imaging in active collaboration with the Department of Otolaryngology, Sher-e-Bangla Medical College and Hospital (SBMCH), Barishal, Bangladesh, spanning January 1 to December 31, 2025. A consecutive recruitment framework was implemented to enroll N = 126 symptomatic patients referred from inpatient and outpatient otorhinolaryngology services. Eligibility criteria comprised male and female patients aged ≥ 12 years presenting with persistent sinonasal symptoms (≥ 12 weeks duration), acute-on-chronic exacerbations refractory to medical therapy, sinonasal polyposis, or clinically suspected neoplasia requiring multiplanar CT mapping. Baseline cohort exclusion criteria comprised prior extensive sinonasal surgery distorting landmarks, acute maxillofacial trauma, pre-existing confirmed malignancy prior to referral, and pregnancy. Procedurally, all N = 126 patients underwent non-contrast helical MSCT; intravenous contrast administration was selectively reserved for complicated cases, excluding patients with severe renal impairment (eGFR < 30 mL/min/1.73 m² or serum creatinine > 1.5 mg/dL) or iodinated contrast allergy. Institutional Ethics Committee approval (Ref: SBMC/IRB/2024/057) and written informed consent were obtained from all participants or legal guardians alongside minor assent.

Helical examinations were performed on a 128-slice multidetector CT system (120 kVp, 100–150 mAs, automated current modulation, 0.625 mm raw collimation, pitch 0.9–1.0) scanning continuously from the frontal sinus roof to the hard palate. Multiplanar reformations in axial, direct coronal, and sagittal planes were reconstructed at 0.5–1.0 mm thickness and reviewed on calibrated bone (WW 2000–3000 HU, WL 200–400 HU) and soft-tissue display windows (WW 350–400 HU, WL 30–40 HU). Scans were independently evaluated by academic radiologists. Mucosal thickening was defined as > 3 mm, and drainage occlusion as complete ostial soft-tissue filling. Sinonasal variations and drainage patterns were systematically tabulated. Patients belonging to the chronic rhinosinusitis (CRS) sub-cohort (n = 96; CRSsNP n = 66, CRSwNP n = 30) were staged using the standardized Lund-Mackay score (0–24) and categorized into operational, study-specific opacification tiers (mild: 1–6, moderate: 7–12, severe: 13–24). Data were analyzed using IBM SPSS Version 28.0 (Mean ± SD; n, %), with two-tailed $p < 0.05$ denoting statistical significance.

III. RESULTS

A total of N = 126 consecutive symptomatic patients underwent diagnostic evaluation using Multi-Slice Computed Tomography (MSCT). The cohort had a mean age of 34.6 ± 12.4 years (range: 13 to 68 years), peaking in the third (32.5%, n = 41/126) and fourth decades (26.2%, n = 33/126). Male patients predominated (57.9%, n = 73/126; male-to-female ratio 1.38:1). Rural residents accounted for 61.9% (n = 78/126) of the cohort, reflecting the agricultural catchment demographics of the tertiary facility (Table 1).

Table 1: Baseline Sociodemographic and Clinical Characteristics of the Study Cohort (N = 126)

Characteristic / Variable	Frequency (n)	Percentage (%)
Age Categories (Years)		
≤ 20 years	14	11.1%
21 – 30 years	41	32.5%
31 – 40 years	33	26.2%
41 – 50 years	23	18.3%
> 50 years	15	11.9%
Mean Age ± SD (Range)	34.6 ± 12.4 years	(13 – 68 years)
Gender Distribution		
Male	73	57.9%
Female	53	42.1%

Male to Female Ratio	1.38 : 1	—
Place of Residence		
Rural	78	61.9%
Urban / Semi-urban	48	38.1%

**Notes: Total evaluated patient cohort N = 126. Percentages calculated on whole cohort denominator.*

Presenting clinical symptoms were dominated by nasal obstruction or congestion in 77.8% (n = 98/126) of patients. Facial pain, headache, or heaviness was documented in 66.7% (n = 84/126), followed by mucopurulent rhinorrhea in 56.3% (n = 71/126), and post-nasal drip in 38.1% (n = 48/126). Subjective olfactory dysfunction (hyposmia or anosmia) occurred in 22.2% (n = 28/126). Allergic manifestations were noted in 19.0% (n = 24/126), recurrent epistaxis in 10.3% (n = 13/126), and chronic halitosis or pharyngeal irritation in 7.9% (n = 10/126) (Table 2).

Table 2: Clinical Presenting Symptoms of Study Patients (N = 126)

Presenting Symptom / Clinical Complaint	Frequency (n)	Percentage (%)
Nasal Obstruction / Congestion	98	77.8%
Facial Pain / Headache / Heaviness	84	66.7%
Rhinorrhea (Mucoid / Purulent Discharge)	71	56.3%
Post-Nasal Drip (PND)	48	38.1%
Hyposmia / Anosmia (Olfactory Dysfunction)	28	22.2%
Allergic Manifestations (Sneezing, Itching)	24	19.0%
Epistaxis	13	10.3%
Halitosis / Chronic Throat Irritation	10	7.9%

**Notes: Multiple presenting clinical complaints were recorded per patient; percentages do not sum to 100%.*

Volumetric CT analysis revealed a high prevalence of sinonasal anatomical variants. Deviated nasal septum (DNS) was the most frequent variant, identified in 62.7% (n = 79/126) of patients, presenting with right-sided deflection in 30.2% (n = 38/126), left-sided deflection in 26.2% (n = 33/126), and S-shaped deviation in 6.3% (n = 8/126). Concha bullosa occurred in 34.1% (n = 43/126) of cases, presenting unilaterally in 23.0% (n = 29/126) and bilaterally in 11.1% (n = 14/126). Prominent Agger nasi cells were observed in 41.3% (n = 52/126). Critical surgical hazard variants included infraorbital ethmoid (Haller) cells in 14.3% (n = 18/126) and sphenoethmoidal (Onodi) cells in 8.7% (n = 11/126). Paradoxical middle turbinates were found in 11.9% (n = 15/126), enlarged ethmoid bullae in 15.1% (n = 19/126), and uncinate process pneumatization in 6.3% (n = 8/126) (Table 3).

Table 3: Prevalence and Anatomical Distribution of Sinonasal Variations on MSCT (N = 126)

Anatomical Variation / Surgical Landmark	Frequency (n)	Cohort % (n/126)	Subgroup %
Deviated Nasal Septum (DNS)	79	62.7%	100.0%
— Right-sided Deflection	38	30.2%	48.1% of DNS
— Left-sided Deflection	33	26.2%	41.8% of DNS
— S-shaped / Complex Deviation	8	6.3%	10.1% of DNS
Concha Bullosa (Pneumatized Middle Turbinate)	43	34.1%	100.0%
— Unilateral Concha Bullosa	29	23.0%	67.4% of CB
— Bilateral Concha Bullosa	14	11.1%	32.6% of CB
Agger Nasi Cells (Prominent / Enlarged)	52	41.3%	—
Haller Cells (Infraorbital Ethmoid Cells)	18	14.3%	—
Paradoxical Middle Turbinate	15	11.9%	—
Onodi Cells (Sphenoethmoidal Danger Variant)	11	8.7%	—
Enlarged Ethmoid Bulla	19	15.1%	—
Pneumatized Uncinate Process	8	6.3%	—

**Notes: Total cohort denominator N = 126. Onodi cells and Haller cells represent high-risk surgical hazard landmarks requiring explicit pre-operative identification for FESS.*

The anatomical distribution of sinonasal pathology demonstrated marked site predilection. Maxillary sinuses were most frequently involved (80.2%, n = 101/126; bilateral in 57.9%, n = 73/126; unilateral in 22.2%, n = 28/126). Anterior ethmoid involvement occurred in 61.9% (n = 78/126; bilateral in 42.9%, n = 54/126), followed by posterior ethmoids in 42.9% (n = 54/126; bilateral in 30.2%, n = 38/126). Frontal sinus disease was identified in 35.7% (n = 45/126), and sphenoid disease in 22.2% (n = 28/126). Complete pansinusitis opacifying all major sinus cavities was confirmed in 18.3% (n = 23/126) of patients (Table 4).

Table 4: Pattern and Anatomical Extent of Paranasal Sinus Involvement on MSCT (N = 126)

Sinus System & Involvement Pattern	Total Affected (n)	Total %	Unilateral (n, %)	Bilateral (n, %)
Maxillary Sinus	101	80.2%	28 (22.2%)	73 (57.9%)
Anterior Ethmoid Sinus	78	61.9%	24 (19.0%)	54 (42.9%)
Posterior Ethmoid Sinus	54	42.9%	16 (12.7%)	38 (30.2%)

Frontal Sinus	45	35.7%	14 (11.1%)	31 (24.6%)
Sphenoid Sinus	28	22.2%	8 (6.3%)	20 (15.9%)
Pansinusitis Pattern (All Sinuses Affected)	23	18.3%	—	23 (18.3%)

**Notes: Individual sinus involvement categories are non-mutually exclusive. Percentages calculated on N = 126.*

Cross-sectional imaging revealed mucosal thickening exceeding 3 mm as the primary radiological feature in 82.5% (n = 104/126) of patients. Ostiomeatal complex (OMC) occlusion was observed in 56.3% (n = 71/126). Complete cavity opacification was noted in 27.8% (n = 35/126), and polypoid soft-tissue masses in 24.6% (n = 31/126). Retention cysts or mucoceles occurred in 15.9% (n = 20/126), and air-fluid interfaces in 14.3% (n = 18/126). Reactive osseous alterations, including osteosclerosis and remodeling, were detected in 8.7% (n = 11/126). Intrasinus hyperattenuation with microcalcifications suggestive of fungal sinusitis was present in 5.6% (n = 7/126) (Table 5).

Table 5: Major MSCT Radiological Findings and Pathological Patterns (N = 126)

Radiological Feature / Finding on MSCT	Frequency (n)	Percentage (%)
Mucosal Thickening (> 3 mm)	104	82.5%
Ostiomeatal Complex (OMC) Occlusion	71	56.3%
Complete Sinus Cavity Opacification	35	27.8%
Sinonasal Polyposis / Soft Tissue Mass	31	24.6%
Retention Cyst / Sinus Mucocele	20	15.9%
Air-Fluid Interface / Exudative Level	18	14.3%
Osseous Changes (Hyperostosis / Sclerosis / Thinning)	11	8.7%
High-Attenuation / Calcific Foci (Fungal Sinusitis)	7	5.6%

**Notes: Findings are non-mutually exclusive. High-attenuation intrasinus foci represent radiological indicators of fungal colonization or allergic fungal rhinosinusitis.*

Among patients belonging to the chronic rhinosinusitis (CRS) sub-cohort (n = 96), quantitative Lund-Mackay CT scoring yielded a mean opacification score of 10.8 ± 4.2 (range: 2 to 22). Moderate opacification extent (scores 7–12) predominated, accounting for 49.0% (n = 47/96) of evaluated cases. Severe sinus opacification (scores 13–24) was observed in 29.2% (n = 28/96), whereas mild opacification (scores 1–6) occurred in 21.9% (n = 21/96) of the CRS sub-cohort (Table 6).

Table 6: Lund-Mackay CT Opacification Scoring within the Chronic Rhinosinusitis Sub-cohort (n = 96 of N = 126)

Lund-Mackay Opacification Tier	Score Range	Frequency (n)	Percentage (%)
Mild Opacification Extent	1 – 6	21	21.9%
Moderate Opacification Extent	7 – 12	47	49.0%
Severe Opacification Extent	13 – 24	28	29.2%
Total Evaluated CRS Sub-cohort	**1 – 24**	**96**	**100.0%**
Mean Lund-Mackay Score ± SD	**Range: 2 – 22**	**10.8 ± 4.2**	—

**Notes: Evaluated exclusively in patients belonging to the chronic rhinosinusitis (CRS) sub-cohort (n = 96; comprising CRSsNP n = 66 and CRSwNP n = 30; excluding non-inflammatory masses, fungal mycetomas, and isolated retention cysts). Score categorization (mild: 1–6, moderate: 7–12, severe: 13–24) represents operational, study-specific radiological opacification tiers used for analytical stratification, rather than clinically validated prognosis or symptom severity staging. Severe category percentage mathematically verified: 28/96 = 29.2%.*

The final radiological spectrum categorized sinonasal conditions into distinct pathological entities across the cohort (N = 126, Figure 1). Chronic non-specific rhinosinusitis was the primary diagnosis in 52.4% (n = 66/126) of patients, followed by sinonasal polyposis in 23.8% (n = 30/126; comprising antrochoanal polyp in 10.3% and diffuse ethmoidal polyposis in 13.5%). Acute or subacute exacerbations accounted for 7.1% (n = 9/126), fungal rhinosinusitis for 6.3% (n = 8/126), sinonasal mucoceles for 5.6% (n = 7/126), benign neoplasms (osteoma and inverted papilloma) for 3.2% (n = 4/126), and malignant lesions with frank bone erosion for 1.6% (n = 2/126). Laterality evaluation demonstrated bilateral disease in 69.0% (n = 87/126) and unilateral pathology in 31.0% (n = 39/126). Polysinusitis involving multiple sinus pairs represented the predominant opacification pattern, identified in 67.5% (n = 85/126), while monosinusitis was restricted to 14.3% (n = 18/126).

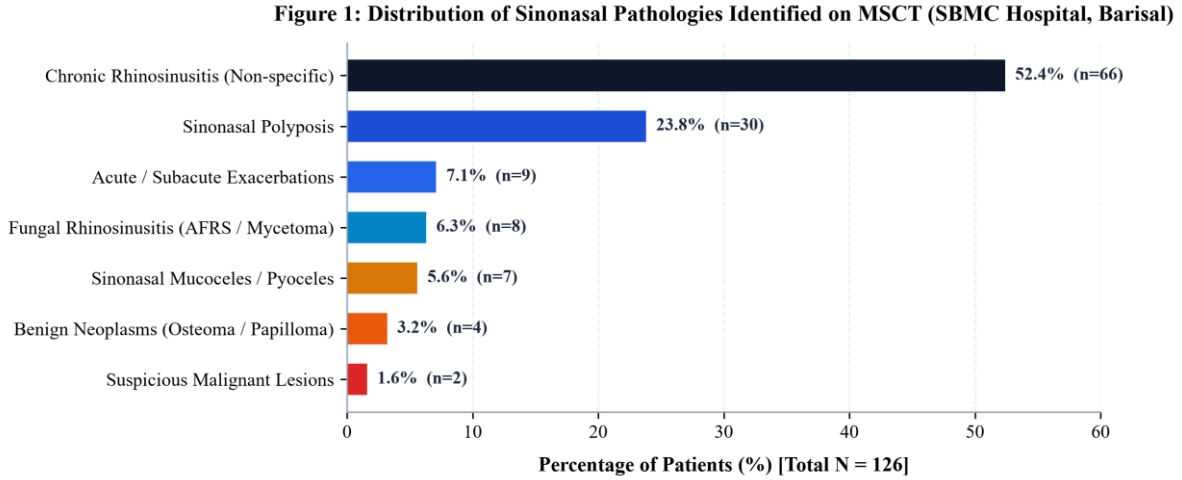


Figure 1: Distribution of primary presumptive radiological and clinico-pathological diagnostic categories across the study cohort (N = 126).

Note: Categories represent mutually exclusive primary diagnostic classifications based on consensus multiplanar MSCT assessment and available clinical records (summing to 100.0%). Definitive histopathological confirmation was restricted to patients undergoing subsequent endoscopic or open surgical excision.

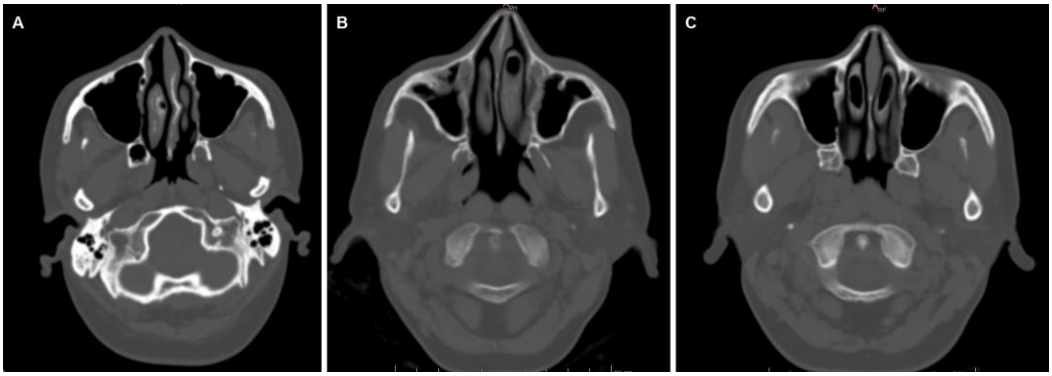


Figure 2: Representative axial MSCT bone windows of sinonasal anatomical variations. (A) Leftward deviated nasal septum with bony spur. (B) Unilateral (left) concha bullosa narrowing middle meatus. (C) Bilateral concha bullosa with intact cortical walls.

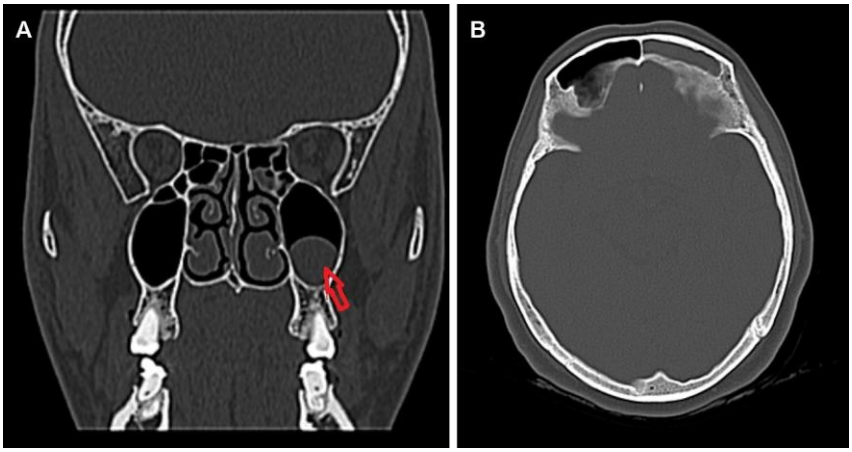


Figure 3: Representative MSCT multiplanar images of sinonasal pathologies. (A) Coronal view showing left maxillary mucosal retention cyst (red arrow). (B) Axial view showing left frontal sinusitis with complete fluid opacification.

IV. DISCUSSION

This hospital-based, descriptive cross-sectional investigation delineates the radiological spectrum of paranasal sinus pathologies and anatomical variations in a tertiary referral cohort from southern coastal Bangladesh, utilizing Multi-Slice Computed Tomography (MSCT) with standardized Lund-Mackay staging. The primary empirical finding reveals a substantial disease burden dominated by chronic inflammatory pathologies, with maxillary (80.2%) and anterior ethmoid (61.9%) sinuses exhibiting the highest vulnerability. The frequent documentation of critical anatomical variations, including deviated nasal septum (62.7%), concha bullosa (34.1%), Agger nasi cells (41.3%), and high-risk surgical landmarks such as Haller cells (14.3%) and Onodi cells (8.7%), reinforces the clinical necessity of pre-operative cross-sectional mapping prior to Functional Endoscopic Sinus Surgery (FESS) [10, 11].

The sociodemographic distribution observed in this cohort—characterized by a mean age of 34.6 ± 12.4 years, peak incidence in the third and fourth decades (58.7%), and modest male predominance (57.9%)—is consistent with epidemiological reports from South Asia and international centers [4, 13]. The rural preponderance (61.9%) mirrors the clinical catchment of Sher-e-Bangla Medical College Hospital in Barishal, which serves a largely agricultural and riverine population. While formal occupational and environmental exposure metrics were not systematically gathered in this cross-sectional study, regional epidemiological literature has hypothesized that prolonged inhalation of agricultural dust, biomass cooking smoke, and untreated allergic rhinitis may represent potential environmental co-factors contributing to upper airway mucosal inflammation in rural South Asian communities [3, 14]. However, given the descriptive cross-sectional design of this study, direct causal relationships between specific environmental exposures, presentation delay, and radiological severity cannot be established. Future prospective analytical investigations incorporating standardized exposure questionnaires and environmental monitoring are warranted to evaluate these potential associations.

Clinical presentations were dominated by nasal obstruction (77.8%), facial headache or heaviness (66.7%), and mucopurulent rhinorrhea (56.3%). While these symptoms represent classical diagnostic criteria under international rhinosinusitis consensus statements [1, 2], our observations emphasize a marked discordance between clinical manifestations and the true anatomical extent of pathology, particularly in deeper posterior ethmoid (42.9%) and sphenoid (22.2%) sinus compartments. Anterior rhinoscopy and physical examination frequently underestimate disease in these posterior air cells [6, 7]. Multi-Slice CT resolves this diagnostic disparity, ensuring comprehensive architectural evaluation and preventing incomplete surgical clearance [15].

The high prevalence of anatomical variants documented in this cohort aligns with global literature, yet specific structural variants carry critical implications for surgical navigation and complication avoidance. Deviated nasal septum (62.7%) and pneumatized middle turbinates (concha bullosa, 34.1%) create mechanical bottlenecks that narrow the middle meatus and ethmoid infundibulum, impeding physiological mucociliary clearance and perpetuating chronic sinusitis [5, 8]. Agger nasi cells, identified in 41.3% of patients, directly abut the frontal recess; their hyperpneumatization narrows the frontal drainage pathway, predisposing to recalcitrant frontal sinus opacification [16]. Crucially, infraorbital ethmoid (Haller) cells (14.3%) project along the medial orbital floor, directly constricting the maxillary sinus ostium and contributing to persistent maxillary disease [17]. Most importantly, sphenoethmoidal (Onodi) cells were detected in 8.7% of patients. Because Onodi cells pneumatize superolaterally around the optic nerve canal and internal carotid artery, failure to identify this variation on pre-operative coronal and axial CT scans exposes patients to devastating intraoperative hazards, including optic nerve transection, irreversible visual loss, and fatal vascular laceration during posterior ethmoidectomy [10, 11]. In addition to ethmoidal variants, cross-sectional evaluation of the cribriform plate height and olfactory fossa architecture according to Keros depth criteria remains vital for skull base integrity. Deep Keros Type III olfactory fossae feature an elongated, fragile lateral lamella of the cribriform plate, rendering this site exceptionally vulnerable to inadvertent penetration during uncinate dissection or anterior ethmoid clearance [8, 14]. Clear pre-operative notation of the Keros type and olfactory fossa asymmetry alerts endoscopic surgeons to this critical hazard zone.

Maxillary sinus involvement was the most frequent finding (80.2%), predominantly bilateral (57.9%), followed by anterior ethmoid (61.9%) and posterior ethmoid (42.9%) sinuses. This anatomical hierarchy corresponds directly to the functional drainage pathway, where the maxillary sinus ostium, situated high on the superomedial wall, relies on upward mucociliary transport through a patent ostiomeatal complex (OMC) [18]. The high frequency of OMC occlusion (56.3%) in our cohort directly correlates with the observed maxillary and anterior ethmoid disease burden. Pansinusitis occurred in 18.3% of patients, indicating advanced, diffuse disease. Mucosal thickening (> 3 mm) was the most common radiological sign (82.5%), while complete cavity opacification (27.8%) and polyposis (24.6%) reflected chronic inflammatory progression. Intrasinus hyperattenuation with microcalcifications, observed in 5.6% of cases, provided diagnostic clues for allergic or non-invasive fungal sinusitis, a condition favored by the warm, humid climate of coastal Barishal [20, 21]. Quantitative disease quantification via the Lund-Mackay staging system demonstrated a cohort mean score of 10.8 ± 4.2 among chronic rhinosinusitis patients (n = 96), with 49.0% presenting with moderate and 29.2% with

severe disease. This substantial severity burden reflects delayed tertiary referral and correlates with the need for definitive endoscopic surgical management [12, 19].

Limitations of the Study

Several methodological limitations should be acknowledged. First, the cross-sectional, single-center design at a tertiary academic referral center introduces inherent referral selection bias toward severe or refractory disease, which may overestimate the prevalence of complex pathologies relative to community populations. Second, microbiological and histopathological confirmation was available only for patients undergoing surgical intervention (such as polyposis and suspected fungal disease), whereas outpatient cases were categorized on radiological and clinical criteria. Third, long-term post-operative functional outcomes using validated disease-specific instruments (such as SNOT-22 scores) were not evaluated. Finally, because treatment decisions were based on clinical discretion rather than randomized allocation, unmeasured confounding and indication bias cannot be excluded. Prospective multicenter studies incorporating histopathological correlation and post-operative quality-of-life assessments will provide further validation.

V. CONCLUSION

Multi-Slice Computed Tomography provides comprehensive cross-sectional delineation of paranasal sinus pathologies, identifying mucosal thickening in 82.5% and ostiomeatal complex occlusion in 56.3% of evaluated patients. Volumetric imaging maps crucial anatomical variations, including deviated nasal septum (62.7%), concha bullosa (34.1%), Haller cells (14.3%), and high-risk Onodi cells (8.7%). These anatomical landmarks establish a valuable pre-operative anatomical roadmap that assists in mitigating iatrogenic orbital and skull base complications during Functional Endoscopic Sinus Surgery. The Lund-Mackay CT staging system reliably quantifies inflammatory severity, demonstrating a mean score of 10.8 ± 4.2 among chronic rhinosinusitis patients.

Recommendations

Clinical practice guidelines should mandate pre-operative MSCT for all candidates undergoing Functional Endoscopic Sinus Surgery to ensure thorough anatomical mapping. Surgical protocols should incorporate a structured radiological checklist documenting critical danger variants—particularly Onodi cells, Haller cells, and olfactory fossa depth—to minimize surgical complications. Healthcare systems in high-burden coastal regions should prioritize low-dose volumetric CT protocols over conventional plain radiography for refractory rhinosinusitis. Future prospective multicenter registries integrating cross-sectional imaging metrics with long-term patient-reported outcome measures will enhance operative safety and patient care.

DECLARATIONS

Ethical Approval and Consent to Participate: Institutional Review Board / Ethics Committee approval was obtained from the Institutional Ethics Committee (IEC) / Institutional Review Board (IRB) of Sher-e-Bangla Medical College and Hospital, Barishal (Approval Reference No: SBMC/IRB/2024/057) in accordance with the Declaration of Helsinki (1975 revision and its later amendments). Written informed consent was obtained from all individual participants (or their legal guardians) prior to enrollment.

Consent for Publication: Not applicable. The manuscript does not contain any individual person's identifiable data or images in any form.

Availability of Data and Materials: The datasets generated and analyzed during the current study are available from the corresponding author on reasonable academic request.

Competing Interests: The authors declare that they have no financial, commercial, or professional conflicts of interest regarding the publication of this manuscript.

Funding: This research received no specific grant from any funding agency in the public, commercial, or not-for-profit sectors.

Authors' Contributions: Dr. Hawa Begum: Conceptualization, study design, radiological investigation, formal analysis, manuscript drafting, and supervision. Biplob Mondal, Rafeza Khanom, Mithun Bahadur, Sabbir Hossen: Data curation, image validation, literature review, and critical manuscript revision. All authors read and approved the final submitted manuscript.

REFERENCES

[1]. Fokkens WJ, Lund VJ, Hopkins C, Hellings PW, Kern R, Reitsma S, et al. European Position Paper on Rhinosinusitis and Nasal Polyps 2020. Rhinology. 2020;58(Suppl S29):1-464. doi:10.4193/Rhin20.600

[2]. Orlandi RR, Kingdom TT, Smith TL, Bleier B, DeConde A, Luong AU, et al. International consensus statement on allergy and rhinology: rhinosinusitis 2021. Int Forum Allergy Rhinol. 2021;11(3):213-739. doi:10.1002/alr.22741

[3]. Bhattacharyya N. The economic burden and symptom manifestations of chronic rhinosinusitis. Am J Rhinol. 2003;17(1):27-32.

[4]. Dua K, Chopra H, Khurana AS, Munjal M. Computed tomographic imaging of paranasal sinuses. Indian J Otolaryngol Head Neck Surg. 2005;57(3):252-256.

[5]. Stammberger HR, Kennedy DW. Paranasal sinuses: anatomic terminology and nomenclature. The Anatomic Terminology Group. Ann Otol Rhinol Laryngol Suppl. 1995;167:7-16.
[6]. Connor SE, Leung R, Woodcock VJ. Development of a low-dose computed tomography protocol for paranasal sinus imaging: a comparison with plain radiography. Clin Radiol. 2008;63(7):787-794. doi:10.1016/j.crad.2007.12.010
[7]. Stankiewicz JA, Chow JM. A cost analysis of the surgical treatment of chronic rhinosinusitis: endoscopy versus CT scan. Am J Rhinol. 2003;17(3):139-142.
[8]. Earwaker J. Anatomic variants in sinonasal CT. Radiographics. 1993;13(2):381-415. doi:10.1148/radiographics.13.2.8460226
[9]. Lloyd GA. CT of the paranasal sinuses: normal anatomy. In: CT of the Paranasal Sinuses: Study of a Normal Population and Clinical Implications. Berlin: Springer; 1990. p. 1-18.
[10]. Stankiewicz JA, Lal D, Connor M, Welch K. Complications in endoscopic sinus surgery for chronic rhinosinusitis: a 25-year experience. Laryngoscope. 2011;121(12):2684-2690. doi:10.1002/lary.21446
[11]. Sarna B, Bansal T. Anatomical variations in paranasal sinuses on multidetector computed tomography. Int J Otorhinolaryngol Head Neck Surg. 2018;4(2):473-478.
[12]. Lund VJ, Mackay IS. Staging in rhinosinusitis. Rhinology. 1993;31(4):183-184.
[13]. Kayalioglu G, Oyar O, Govsa F. Nasal cavity and paranasal ethmoidal cells: a computed tomography study. Rhinology. 2000;38(4):175-179.
[14]. Keros P. On the practical value of differences in the level of the lamina cribrosa of the ethmoid. Z Laryngol Rhinol Otol. 1962;41:809-813.
[15]. Hopkins C, Browne JP, Slack R, Lund VJ, Topham J, Reeves B, et al. The Lund-Mackay staging system for chronic rhinosinusitis: how is it used and what does it tell us? Otolaryngol Head Neck Surg. 2007;137(4):555-561.
[16]. DelGaudio JM, Hudgins PA, Venkatraman G, Beningfield A. Multiplanar computed tomography analysis of frontal recess cells in patients with chronic frontal sinusitis. Am J Rhinol. 2005;19(4):347-353.
[17]. Melroy CT, Senior BA. Sinonasal anatomy: the essentials. Otolaryngol Clin North Am. 2008;41(1):1-14.
[18]. Yousem DM. Imaging of sinonasal inflammatory disease. Radiology. 1993;188(2):303-314.
[19]. Dasar U, Gokce E. Evaluation of variations in sinonasal region with multidetector CT. Eur J Radiol Open. 2016;3:98-108.
[20]. Mukherji SK, Figueroa RE, Ginsberg LE, Zeifer BA, Marple BF, Alley JG, et al. Allergic fungal rhinosinusitis: CT findings. Radiology. 1998;207(2):417-422.
[21]. Alkire BC, Bhattacharyya N. An assessment of the diagnoses of chronic rhinosinusitis and chronic rhinitis in the United States. Laryngoscope. 2008;118(8):1478-1481.